Faraday Discussions

Accepted Manuscript

This manuscript will be presented and discussed at a forthcoming Faraday Discussion meeting. All delegates can contribute to the discussion which will be included in the final volume.

Register now to attend! Full details of all upcoming meetings: http://rsc.li/fd-upcoming-meetings

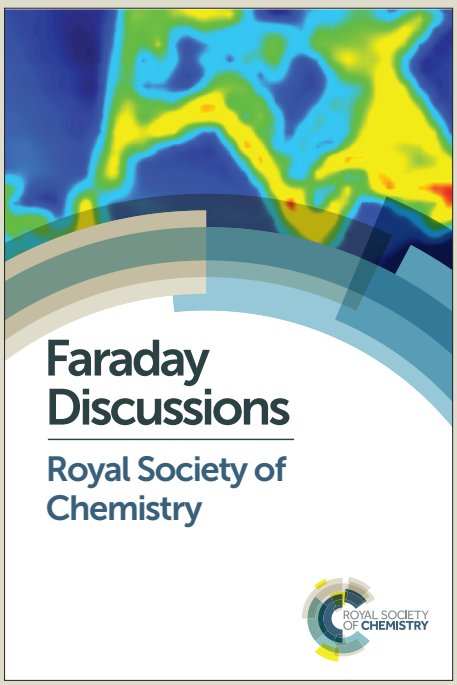

This is an *Accepted Manuscript*, which has been through the Royal Society of Chemistry peer review process and has been accepted for publication.

Accepted Manuscripts are published online shortly after acceptance, before technical editing, formatting and proof reading. Using this free service, authors can make their results available to the community, in citable form, before we publish the edited article. We will replace this *Accepted Manuscript* with the edited and formatted *Advance Article* as soon as it is available.

You can find more information about *Accepted Manuscripts* in the Information for Authors.

Please note that technical editing may introduce minor changes to the text and/or graphics, which may alter content. The journal's standard Terms & Conditions and the Ethical guidelines still apply. In no event shall the Royal Society of Chemistry be held responsible for any errors or omissions in this *Accepted Manuscript* or any consequences arising from the use of any information it contains.

ROYAL SOCIETY OF CHEMISTRY

www.rsc.org/faraday_d

Acetylene hydrogenation over structured Au-Pd catalysts

Alan J. McCue[1]*, Richard T. Baker[2] and James A. Anderson[1]*

[1]Surface Chemistry and Catalysis Group, Materials and Chemical Engineering,

School of Engineering, University of Aberdeen, Aberdeen, UK, AB24 3UE.

[2]School of Chemistry, University of St Andrews, St Andrews, UK, KY16 9ST

Fax: +44 1224 272901, Tel: +44 1224 272838, Email: a.mccue@abdn.ac.uk, j.anderson@abdn.ac.uk

Abstract

AuPd nanoparticles were prepared following a methodology designed to produce core-shell structures (Au core and Pd shell). Characterisation suggested slow addition of the shell metal favoured deposition onto the pre-formed core, whereas more rapid addition favoured the formation of a monometallic Pd phase in addition to some nanoparticles with core-shell morphology. When used for the selective hydrogenation of acetylene, samples which possessed monometallic Pd particles favoured over-hydrogenation to form ethane. A sample prepared by slow addition of a small amount of Pd resulted in the formation of a core-shell structure but with an incomplete Pd shell layer. This material exhibited completely different product selectivity with ethylene and oligomers forming as the major products as opposed to ethane. The improved performance was thought to be as a result of the absence of Pd particles which were capable of forming a Pd-hydride phase with enhanced oligomer selectivity associated with reaction on uncovered Au atoms.

Keywords

Selective hydrogenation, acetylene, AuPd bimetallic catalyst, nanoparticles, core-shell

Introduction

Olefin manufacture *via* naphtha cracking yields alkene streams containing small quantities of alkyne impurities which require removal to avoid complications with downstream polymerisation steps. The preferred industrial route is *via* selective hydrogenation of the alkyne since this yields additional alkene.[1,2,3] This is generally accomplished over a bimetallic catalyst with Pd acting as the active metal and Ag as a structural modifier.[4] Achieving high selectivity at close to complete alkyne conversion remains difficult as the alkene has unhindered access to the catalyst's surface so can readily adsorb and react to give undesired alkane. CO is often co-fed as a transient poison to

compete with alkene for adsorption sites, although the amount added must be carefully regulated depending on catalyst activity.[2] This process has been widely studied since the pioneering works of Bond and Wells,[5] however, recent advances in experimental techniques and computational methodologies have resulted in an increased understanding of the factors which promote over-hydrogenation. Over a monometallic Pd catalyst, it is now thought that the interplay between Pd hydride and carbide phases governs alkene selectivity.[6,7,8,9,10,11,12,13,14,15] It has also been shown that alloying Pd with Ag minimises hydride formation resulting in increased alkene selectivity.[16]

A number of strategies have been explored in recent years to improve selectivity over Pd catalysts,[17,18,19] or even circumvent the need for Pd.[20,21,22] For example, the selectivity of Pd catalysts can be significantly improved by adsorption of organic modifiers[23,24,25,26,27] onto the metal surface which is thought to create sites which favour acetylene adsorption while hindering adsorption of ethylene. Whilst industrial catalysts typically use Ag as a structural modifier, a number of other metals have been explored.[28,29,30] In general, improved alkene selectivity occurs when hydride formation is minimised, although a growing number of reports suggest that Pd atom isolation is beneficial.[31,32,33] A number of alternative metals such as Cu,[34,35] Ag[36,37] and Au[38] offer inherently better selectivity than Pd but require operation at relatively high temperatures (*ca*. 523 K) since hydrogen dissociation is restricted by an activation energy barrier. Such temperatures significantly exceed those used by current industrial reactors (approx. 313-413 K) which may limit potential implementation. To overcome this limitation, attempts have been made to increase the activity of Cu catalysts by adding small quantities of Pd to act/create sites which permit hydrogen dissociation at low temperature (*ca*. 373 K).[39,40,41,42,43,44,45,46] Recent literature reports hint that a similar approach may be achieved by addition of Pd to Ag[47] and Au[48] catalysts. Metal free ceria has also been shown to be extremely selective for acetylene and methylacetylene hydrogenation but requires operation at high temperature (> 473 K).[49] This can be overcome by doping with Ga which appears to create sites which allow for hydrogen dissociation at lower temperature,[50] although no data based on operation at elevated pressure is available.

The ability to synthesise bimetallic nanoparticles has advanced rapidly in recent years with significant attention devoted to AuPd nanoparticles.[51,52] These materials often possess unique structure/order on the nanoscale (i.e., the manner in which the two metals interact is controlled). For example Ma *et al*.[53] compared the performance of AuPd octahedra with nanoflowers (organised agglomerates of the octahedra) and identified that the nanoflower samples exhibited superior performance for the selective hydrogenation of acetylene. One particular class of bimetallic nanomaterial which attracts particular attention are core-shell nanoparticles,[54,55] where one metal

forms a shell over the second metal. In principle, when the shell is relatively thin, the electronic properties of the shell metal may be perturbed which offers exciting possibilities with regards to adsorption and catalytic behaviour.[56,57,58] In-spite of the obvious appeal, synthesis methods rarely seem to produce only core-shell nanoparticles. Instead, a mixture of core-shell, bimetallic and monometallic particles are often formed making evaluation of the catalytic properties of individual species challenging.[59] Additional complications arise from the synthesis methods employed with stabilising agents such as polyvinylpyrrolidone necessary to avoid nanoparticle agglomeration. If the polymer is not removed, these can influence catalytic performance, although sometimes for the better.[60,61] Various removal methods have been explored including ozone/UV radiation[62] and solvent treatments;[63] however moderate to high temperature calcination still remains the most common method. This may not be appropriate for core-shell structures since the two metal components are likely to mix resulting in the loss of the unique structure.[64]

A recent report by Wilson *et al.*[64] described a synthesis method where core-shell AuPd structured nanoparticles could be synthesised with different Pd shell thickness with EDX-STEM and FTIR of adsorbed CO results consistent with this assumption. In this study, use of this synthesis method is made and this preparation methodology is further explored by adding different amounts of Pd to pre-formed Au nanoparticles. Results indicate that nanoparticle structure and catalytic performance varies considerably depending on Pd loading.

Experimental

Catalyst preparation

Nanoparticles with assumed Au cores and Pd shells of different thickness were prepared by following the procedure of Wilson *et al.*[64] with minor modification. This method has been shown to result in core-shell nanoparticles with Pd shell thickness controllable to some extent by adding different amounts of Pd. Briefly, Au nanoparticles were synthesised by reduction of an aqueous solution of $HAuCl_4$ with pre-chilled $NaBH_4$ to yield a red sol. Hydroquinone was subsequently added to the mixture before an aqueous solution of Na_2PdCl_4 was added at a constant rate *via* a syringe pump (Table 1) with the intention of depositing Pd onto the pre-formed Au nanoparticles. Following complete addition of the Pd solution, the reaction was quenched by adding aqueous HCl and the nanoparticles stabilised with polyvinylpyyrolidone (PVP). The nanoparticles were immobilised onto a support by adding an appropriate portion of the metal solution to an aqueous slurry of TiO_2 (P25, Evonik, acidified with H_2SO_4) to give a 1 wt% loading. Finally, the solid was filtered, washed thoroughly with ultrapure water, dried at 60°C and stored in this state prior to use. Following this

methodology, 3 samples were prepared with different amounts of Pd and Au (Table 1). Samples are denoted as xPd(Au) with 'x' indicating the nominal Pd:Au atomic ratio. Significantly, samples were not subjected to high temperature calcination which may change the surface composition by allowing for metal mixing or preferential segregation.[59,64] This does mean, however, that samples will have retained some PVP on the surface. In order to investigate the significance of this, samples were pre-treated in hot water and water/UV-light which have been shown to be effective in removing PVP to some extent.[62,63] Monometallic samples (1 wt% Pd or Au) were also prepared by reduction of the appropriate metal with $NaBH_4$ followed by immobilisation onto the same TiO_2 support for comparison purpose.

Catalyst testing

Catalysts were tested for activity/selectivity in the gas phase hydrogenation of acetylene using a Microactivity reference reactor (PID Eng & Tech, supplied by Micromeritics). Approximately 200 mg of sample was diluted with 800 mg SiC and supported in a 9 mm i.d. stainless steel reactor. Prior to reaction, samples were reduced in 30% H_2/N_2 for 1 h at 373 K. The relatively low reduction temperature was deliberately chosen to avoid perturbation of the surface composition. Reactions were typically performed at 1 bar using a mixture of 0.6% acetylene/1.1% hydrogen/balance N_2 to give a H_2:acetylene ratio of 1.8:1 and a space velocity of 24000 h^{-1}. The main reaction parameter varied was temperature (323-363 K) with 5 h time on stream permitted at each condition to ensure catalysts stabilisation. One run was conducted with a 3.6:1 H_2:acetylene ratio. Analysis of the effluent gas was performed using a PE Clarus 580 GC fitted with an FID and a 30 m x 0.53 mm elite alumina capillary column. Acetylene conversion was calculated as the amount reacted divided by the amount introduced. Selectivity to ethylene and ethane was calculated as the amount formed divided by the amount of acetylene reacted and selectivity to oligomers was calculated based on a carbon balance. Under these conditions full acetylene conversion was generally achieved which makes the extraction of kinetic parameters inappropriate. These conditions allow for assessment of ethylene selectivity under challenging conditions which mirror industrial requirements (< 5 ppm acetylene in effluent gas).

Characterisation

TEM images were obtained using a JEOL JEM 2011 instrument operating with a LaB_6 filament at an accelerating voltage of 200 kV and equipped with an Oxford Instruments EDS spectrometer. The images were captured using a Gatan CCD camera and analysed using Digital Micrograph 3.4.4 software. This software was also used to prepare Digital Diffraction Patterns (DDPs) by applying

Fourier transforms to specific regions of the TEM images. The TEM instrument was also used to obtain EDS spectra and to record two-dimensional elemental distribution maps. For TEM examination, the samples were deposited from suspension onto holey carbon-coated Cu grids. TiO_2-supported samples were deposited from suspension in acetone. Unsupported nanoparticles were prepared as described earlier, but were additionally subjected to centrifugation and washed with ultrapure water before being suspended in aqueous media and deposited onto grids. A few images were obtained from grids prepared from sample suspensions prior to centrifugation and washing but these proved unstable in the microscope because of the effect on the grids of dissolved HCl and the formation of salt crystals. In order to avoid the effects of these impurities (*e.g.* overlap of the Cl and Pd spectra) and compositional segregation effects during centrifugation, EDS spectra of the supported nanoparticle samples were used to calculate the Pd:Au ratios presented below.

Temperature programmed reduction (TPR) experiments were conducted on a TPDRO 1100 instrument with a TCD detector using a 5% H_2/N_2 mixture. Profiles were collected over a temperature range of 313-373 K using a heating rate of 5 K min^{-1} and signal output normalised per gram of sample. CO pulse chemisorption experiments were carried out on the same instrument to evaluate CO uptake. Samples were reduced at 373 K for 1 h before being cooled to 308 K. Diluted CO (19% in He) was pulsed (0.285 ml loop volume) over the sample until saturation was attained.

FTIR of adsorbed CO was performed using a PE Spectrum 100 spectrometer with sample presented as a 16 mm diameter self-supporting disc. The disc was suspended in a quartz holder and held in a vacuum system which permitted *in situ* evacuation and gas manipulation. The sample was initially outgassed before being reduced in 50 ml min^{-1} H_2 at 373 K for 1 h (note: same pretreatment temperature as used for catalytic measurements). The sample was cooled and the system evacuated to *ca.* $4x10^{-5}$ mbar. An initial spectrum (25 scans, 4 cm^{-1} resolution) was collected prior to stepwise introduction of increasing CO overpressures (0.1-40 Torr) at beam temperature. Results are presented as difference spectra using a scan before exposure to CO as background. Spectra collected following this approach generally exhibited weak absorption bands (likely due to the presence of PVP on the surface blocking sites) but the bands due to CO observed subsequently reflect the surface sites present available during catalytic measurements.

Results

Synthesis and characterisation

The synthesis of bimetallic AuPd nanoparticles is known to be complex with composition often varying depending on metal particle size when both metals are introduced simulatenously.[51,52]

There are numerous groups who have reported preparation methods which produce nanoparticles with gold cores and palladium shells,[56,57,58,59,64] however, these often form in addition to monometallic particles and bimetallic particles where the two metals are mixed/alloyed. In this work, the synthesis method reported by Wilson *et al.*[64] was adopted which appeared to produce core-shell nanoparticles based on the characterisation presented.[64] In order to synthesise samples, 3 equivalent Au colloidal solutions were prepared before different amounts of Na_2PdCl_4 was added at different rates (Table 1), followed by deposition onto a TiO_2 support. A material, designated as 0.2Pd(Au), was prepared by adding a small amount of Pd (0.1 wt% once supported) at a very slow addition rate (5 µmol h^{-1}). Under these conditions, the concentration of total palladium in solution is expected to be very low meaning that formation of monometallic Pd particles is unlikely (i.e., Pd is more likely to deposit onto the existing Au particles). The Pd:Au ratio estimated by EDS for this sample was 0.26 which correlates well with the nominal ratio of 0.20 (Table 1). Interestingly, Wilson *et al*. determined a Pd:Au ratio of 0.23 by ICP-MS for an equivalent material and highlighted that such low Pd loadings are likely to result in less than monolayer coverage of the Au core.[64] Dynamic pulse chemisorption of CO was useful for gaining an understanding of the number of Pd surface sites because, under these conditions, CO adsorption on a monometallic Au sample was negligible (Table 1). CO uptake for this sample was 2.2 µmol g^{-1} (Table 1), lower than expected based on the amount of Pd added (CO:Pd ratio = 0.2) which implies that at least a fraction of Pd is inaccessible due to covering by PVP.

A second sample, denoted as 1.5Pd(Au), was prepared by adding a larger amount of Pd (0.45 wt% once supported) at an addition rate of 36 µmol Pd h^{-1}. The Pd:Au ratio determined by EDS for this sample was 0.80 which falls below the nominal ratio (1.5) and may be as a result of incomplete reduction of the Pd precursor and subsequent loss during filtration and washing steps. CO chemisorption resulted in 6.6 µmol g^{-1} uptake and a CO:Pd ratio of 0.2 assuming the nominal Pd loading. 1.5Pd(Au) has a higher Pd loading than 0.2Pd(Au) but an equivalent CO:Pd ratio and this is tentatively taken as evidence of multilayer deposition on the Au core (i.e., not all of the Pd present are surface sites). However, given that Pd was added more rapidly, the concentration of Pd species in solution during synthesis is expected to be higher which enhances the probability of forming monometallic Pd clusters/nanoparticles. A third sample, 3.3Pd(Au), was prepared and had the highest nominal Pd loading (0.65 wt% once supported) and Pd addition rate (57 µmol g^{-1}). Characterisation of this sample (presented later) suggests that some nanoparticles may be 'Pd rich' or even exclusively contain Pd. The Pd:Au ratio obtained by EDS is lower than expected (1.1 *vs* 3.2 – see Table 1) and again incomplete reduction of Pd is thought to be the cause (note: Wilson *et al*. also reported lower Pd:Au than nominal ratios).[64] CO uptake for this sample was 5.3 µmol g^{-1} which

corresponds to a CO:Pd ratio of only 0.09 (based on the nominal Pd loading) which implies that not all Pd atoms can be surface atoms. This is consistent with both multilayer formation around Au cores and the presence of monometallic Pd particles.

Following deposition of the nanoparticles onto TiO_2 they were thoroughly washed with water to remove as much of the PVP stabilising agent as possible. DRIFTS spectra of the supported nanoparticles following drying confirm the presence of PVP on the surface (bands at 2960, 2924, 2880 and 2868 cm^{-1} due to the CH_3 asymmetric, CH_2 asymmetric, CH_3 symmetric and CH_2 symmetric stretching modes, respectively). Whilst it is desirable to remove the PVP to enable relationship between exposed sites and catalyst performance to be determined, it did not appear to have a significant effect on catalytic measurements (see later). Wilson *et al*.[64] treated samples post synthetically at 573 K to remove the remaining PVP but this (intentionally) resulted in the two metals mixing. Given that the aim of this work was to access the impact of the Pd shell thickness on catalytic performance, treatments which induce metal mixing are undesirable. The effectiveness of a lower temperature calcination step (373-473 K) was evaluated, although no evidence of PVP decomposition/loss was apparent as assessed by DRIFTS. Instead, alternative methods were explored for comparison purpose. The 'hot-water' method reported by Lopez-Sanchez *et al*.[63] to be effective for partial dissolution of polyvinylalcohol was tested along with irradiation of samples dispersed in water with UV light. Both methods appeared successful in exposing additional metal sites, although the intensity of C-H stretching modes did not decrease significantly suggesting some PVP was retained.

One method which can be used to evaluate whether monometallic Pd particles exist within a sample is temperature programmed reduction (TPR). Exposure of Pd to hydrogen at room temperature leads to the formation of a hydride phase which decomposes above ambient temperature producing a characteristic negative peak.[14] TPR profiles generated by heating various samples in 5% H_2/N_2 at 5 K min^{-1} from 313 to 373 K are shown in Figure 1 (note: data is presented as detector signal *vs* time to improve clarity). Monometallic Pd prepared by reduction of Na_2PdCl_4 shows a negative feature at 343 K which is attributed to decomposition of β-Pd-hydride. The equivalent profiles for 0.2Pd(Au), 1.5Pd(Au) and 3.3Pd(Au) show no negative feature. Instead, a very gentle increase in detector signal suggests a small degree of reduction as temperature approaches 373 K. As such, the ability to form a hydride phase, as judged by TPR alone cannot be used to rationalise the differences in product selectivity (see later). This may be because the technique is not sufficiently sensitive or that the materials do not possess large enough clusters of Pd to form a hydride phase. Indeed, it is known that hydride formation tends to zero as Pd dispersion increases to 100%.[65]

TEM imaging

Figure 2 presents TEM images taken at a range of magnifications of the unsupported 3.3Pd(Au) nanoparticles deposited onto the TEM grid directly from their native suspension. Despite the adverse effects of the other constituents of this suspension (see Experimental section), these images clearly show the highly dispersed nature of the nanoparticles, their approximately spherical morphology and their uniform diameter, of around 3-4 nm. Crystal planes and atomic columns are evident in the higher magnification images and a DDP was obtained from the nanoparticle circled in Figure 1(f). This was indexed to the face centred cubic crystal structure (space group 225, $Fm\bar{3}m$) expected for both Pd and Au, viewed along the [001] zone axis. Because of the relatively low spatial resolution of DDPs obtained from such small particles, it is unlikely that Pd and Au could be distinguished with confidence on the basis of the difference in their unit cell dimensions (a= 3.89 Å for Pd and a= 4.08 Å for Au, a difference of 4.5%). The most commonly observed spots in DDPs of these metals are the {200} and {111} sets with spacings of 1.95 and 2.04 Å and 2.25 and 2.35 Å for Pd and Au, respectively. Au-Pd core-shell particles would be expected to appear as a light ring with a dark centre in the TEM because of the difference in atomic mass between Pd (106) and Au (197). How clearly, and whether, this is observed depends again on particle size, the relative thicknesses of the core and the shell and on the imaging conditions. In the intermediate magnification images in Figure 2(b), (c) and (d), some of the particles do indeed appear to have a core-shell structure, and some of these are indicated in the figure.

For further imaging, and for elemental analysis by EDS, the nanoparticles were washed and centrifuged to separate them from their native suspension before re-suspending them in deionised water. In these samples, clusters of nanoparticles are typical, such as those shown in Figure 3. EDS mapping allows the spatial distribution of selected elements across the area of interest to be determined in the TEM. Although the nanoparticles were too small for Au and Pd distributions to be mapped within individual nanoparticles, Pd and Au maps were obtained from the clusters shown in Figure 3 for the 3.3.Pd(Au) sample. Both Au and Pd extend throughout the structures seen in the TEM images and, importantly, the distribution of Pd closely matches that of Au. This indicates an intimate mixing of these two elements. It follows that at least most nanoparticles contain both elements. To investigate this further, ED spectra were obtained from further clusters and also from points within clusters, as presented in Figure 4. For 0.2Pd(Au), whole clusters as well as points within clusters were seen to have a consistently high Au and low Pd content (Figure 4(a) and (b)). This was also the case for the majority of clusters of 1.5Pd(Au) and 3.3Pd(Au) –as shown in Figure 4(c) and (f) and for the two nanoparticles shown in Figure 4(g). However, a minority of the particles analysed

were almost pure Pd. This is the case within the circled area of Figure 4(d) and in the expanded view in (e) for 1.5Pd(Au) as well as for the nanoparticles of 3.3Pd(Au) seen in Figure 4(h). The image and DDP in Figure 4(i) confirm the expected crystallography of these particles.

Figures 5 to 7 present, respectively, images of the 0.2, 1.5 and 3.3Pd(Au) nanoparticles supported on titania which were used as catalysts in this work. Nanoparticle size distributions of these samples were determined from the TEM images and are presented in Figure 8. These were very similar for all three samples, each of which showed an average particle size of 3.5 to 3.7 nm. The high dispersion of these nanoparticles across the support is shown for 0.2Pd(Au) in Figure 5(a). In Figure 5(b) a metal particle is viewed in profile and the crystal structure of the nanoparticle and the support each afford complete DDPs. The support can be indexed to the anatase phase of titania viewed along the [100] (or [010]) direction (the presence of the 002 spots – normally systematically absent – suggests either a defective structure or some double diffraction) and the additional spots in DDP(ii) can be assigned to the metal viewed along its [011] zone axis. As is typical of these samples, the crystal lattices of the metal and the support are not aligned. This is consistent with the preparation method, in which nanoparticles are first synthesised and then deposited onto the support. The majority of the nanoparticles are also polycrystalline, exhibiting multiple crystal domains. This is the case for the 7 nm particle in Figure 5(c) and for the singly-twinned particles in (e) and (f). The DDP of the latter contains a full diffraction pattern for the larger domain (on the left) plus additional spots for the smaller domain (right). It was very rare to observe core-shell structures in the nanoparticles supported on titania. One example is the particle shown in profile in Figure 5(d) which has a dark centre and lighter region around it, both clearly facetted. Although more speculative, it is also possible that the nanoparticle in image (e) has a very thin, light shell, of maybe only one atomic layer. The images in Figure 6 show similar results for 1.5Pd(Au). The metal nanoparticles are well dispersed across the surface of the support particles. At high resolution the majority appear to be polycrystalline – as in Figure 6(c), (e) and (f) - and not crystallographically aligned with the support, as shown in the DDP of image (c). Image (d) appears to show two overlapping nanoparticles and in image (f) the very clear twin boundary is indicated. Finally, for 3.3Pd(Au), the low magnification images in Figure 7 again show the dispersion of the metal nanoparticles across the support. At high magnification, the central particle in (c) is multiply-twinned and the DDP of the circled particle in (d) can be indexed to Au or Pd viewed along the [011] direction. No features were seen in the images of the titania-supported samples of either 1.5Pd(Au) or 3.3Pd(Au) which could be identified as core-shell structures.

Catalyst testing

Catalyst testing was conducted in a fixed bed stainless steel reactor under conditions which typically produce high acetylene conversion. Such conditions are beneficial for accessing whether or not a catalyst is prone to over-hydrogenation given that the reaction is essentially a sequential process (i.e., the enthalpy of adsorption of ethylene is lower than the enthalpy of adsorption of acetylene meaning that ethylene will not readily adsorb in the presence of acetylene). Of course, the choice of these conditions makes the evaluation of reaction rates and kinetic parameters inappropriate. Conversion and selectivity data for samples tested at 363 K are shown in Table 2. Monometallic Pd exhibits complete conversion and a product distribution which shows that ethane is the major product (Table 2 – entry 1). These findings are consistent with literature,[8,9,10,15] although a sample made by reduction of Na_2PdCl_4 demonstrated higher ethylene and oligomer selectivity than a sample prepared by impregnation but tested under otherwise similar conditions.[39] In order to ascertain whether or not this was related to the preparation method or residual PVP on the nanoparticle surface, this catalyst was subjected to calcination at 673 K. This thermal pre-treatment had virtually no effect on the product distribution suggesting that surface PVP has little influence on catalytic performance. Monometallic Au (Table 2 – entry 8) was considerably less active (21% conversion) but showed a higher selectivity to ethylene than Pd – again consistent with literature.[38]

3.3Pd(Au) (highest Pd loading) exhibits activity/conversion which is equivalent to monometallic Pd (Table 2 entries 1 and 7). Data collected with 1.5Pd(Au) sample looks almost identical (Table 2 – entry 6). As such, it would appear these samples are dominated by 'Pd like' catalysis. Interestingly, the sample with the smallest Pd loading/shell thickness exhibits completely different catalytic performance. In this case, 0.2Pd(Au) produces ethylene as major product (53%), oligomers as major by-product (41%) and almost no ethane (6%). High activity at only 363 K is a trait associated with Pd whereas high ethylene selectivity is certainly not. This suggests that Pd in this sample is either electronically or geometrically different from the form in which Pd is present in other samples studied in this work. One point of significance is that the oligomer selectivity for 0.2Pd(Au) is abnormally high with respect to Pd. In order to determine whether this was associated with residual PVP on the surface, different pre-treatments were explored with an objective to remove the stabiliser. Treatments in hot water or with UV irradiation (Table 2 – entries 6 and 7, respectively) did not appear to significantly affect oligomer (or any other product) selectivity. From this it is inferred that high oligomer selectivity is not associated with the presence of residual PVP but is more likely associated with some other function related to the exposed metal sites-most likely the presence of Au surface atoms.

Time on stream data for 0.2Pd(Au) sample using 1.8 equivalents of H_2 relative to acetylene (same conditions as used in Table 2) and with a larger 3.6 fold excess of hydrogen is presented in Figure 9. A number of informative points are apparent. Firstly, using 1.8 equivalents of H_2, selectivity is remarkably stable across a range of temperatures with very little tendency to form ethane. For example, ethane selectivity is only increased from 3 to 6% as temperature was raised from 323 to 363 K (even though full acetylene conversion is readily achieved at low temperature). As temperature is increased, the most significant change to selectivity is actually an increase in ethylene selectivity (44 to 53%) at the expense of oligomer formation (53 to 41%). This suggests that oligomer formation is associated with hydrogen availability. Secondly, at low temperature (323 and 333 K), 0.2Pd(Au) is prone to deactivation with a notable decrease in acetylene conversion over 5 h time on stream. This is attributed to the high oligomer selectivity which will eventually lead to a reduction in available adsorption sites. Operation at higher temperature results in the partial recovery of the activity, although most likely masks any further deactivation. Lastly, whilst operation of 0.2Pd(Au) with a slight excess of H_2 relative to acetylene limits over-hydrogenation, use of a larger H_2 excess does result in increased ethane formation, although largely as a result of decreased oligomer formation (Figure 9-b). Under these conditions, deactivation at 323 K is still apparent, although to a lesser extent, again suggesting a correlation between hydrogen availability and oligomer formation. No evidence of deactivation was observed for 1.5Pd(Au) and 3.3Pd(Au) samples (see Supporting information figure 2 and 3, respectively).

FTIR of adsorbed CO

FTIR using CO as a probe molecule is a useful technique for evaluating the nature of surface sites on a supported metal particle since band positions are sensitive to both the type of adsorption site (i.e., type of metal) and the mode of adsorption (e.g. linear *vs* bridge bound CO). FTIR spectra of samples which had been reduced at 373 K and exposed to CO at beam temperature are shown in Figure 10. Following reduction, 0.2Pd(Au) sample exhibits bands at 2071 and 2040 cm^{-1} as well as a contribution from gas phase CO centred at 2143 cm^{-1} (Figure 10-a and b). The band at 2071 cm^{-1} is likely associated with CO adsorbed linearly on Pd corner atoms,[66] although the band position is slightly lower than typically expected suggesting the Pd atoms are electronically perturbed. The broad shoulder at *ca*. 2040 cm^{-1} occurs at frequency seldom observed, although a band at 2050 cm^{-1} has previously been assigned to CO linearly adsorbed on edge sites.[66] Interestingly, there is almost no band intensity in the region where bridge bound CO would be expected (1950-1850 cm^{-1}). Instead, there is only a faint broad band centred at 1920 cm^{-1}, although the intensity is only marginally above instrumental signal to noise in that region. This suggests that very few sites exist

with neighbouring Pd atoms, or that these sites are not available for CO adsorption after reduction at 373 K. Similarly, there is no evidence of a band at *ca*. 2100 cm^{-1} which could be assigned to CO adsorbed linearly on low coordinated Au atoms.[67,68] Again, this implies these sites do not exist (i.e., Pd preferentially occupies low coordination sites) or are not available for adsorption.

In order to ascertain the nature of sites that were blocked by PVP, spectra of adsorbed CO were collected following a UV irradiation/water pre-treatment to remove as much PVP as possible and are presented in Figure 11. Following such a treatment, 0.2Pd(Au) sample (Figure 11-a) presents bands at 2074 and 2037 cm^{-1} which are assigned as before. A much more intense band associated with CO bridging two Pd atoms is apparent at 1970 cm^{-1} (bridging on edge sites) which suggests that PVP does influence surface site availability. However, this appears to have little effect on catalytic performance (compare Table 2 – entries 3 and 5). A further peak is apparent at 2110 cm^{-1} and is attributed to CO linearly adsorbed on Au atoms which correlates well with the vibrational frequency calculated by Zhu *et al*.[69] for CO adsorbed on Au-edge atoms (2112 cm^{-1}) using DFT. The appearance of a band associated with CO adsorption on Au is consistent with sub-monolayer coverage of the Au cores with Pd. As a result, it is thought that 0.2Pd(Au) will possess a number of different surface sites including Pd atoms with only Au neighbours and Pd atoms with one Pd neighbour and further Au neighbours. Importantly, there is no evidence of 3-fold hollow Pd sites which suggests the absence of larger Pd ensembles.

Spectra of 1.5Pd(Au) after reduction at 373 K (Figure 10-b and d) show similarities to those collected for 0.2Pd(Au) sample. Absorption bands are observed at 2070 and 2043 cm^{-1} and correspond to CO adsorbed linearly on Pd atoms as before. However, a far more intense band related to bridge-bound CO on Pd is apparent and is centred at 1936 cm^{-1}. Spectra of this sample following UV/water treatment (Figure 11-b) are only subtly different but highlight two key points. Firstly, no band is observed above 2100 cm^{-1} suggesting the absence of exposed Au atoms. This may be because the Au core is completely covered by Pd atoms (i.e., a true core-shell structure has been formed). Secondly, the region where bridge bound CO is seen is more complex. The centre of the band shifts from 1924 to 1932 cm^{-1} as CO overpressure/coverage is increased. This suggests a degree of dipolar coupling which implies that Pd-Pd dimer sites must be in close proximity to one another. A second feature begins to become resolved at 1969 cm^{-1} which is likely associated with bridge bound CO on Pd edge sites.[66] Finally, the band tails considerably towards lower wavenumber which hints that some 3-fold hollow adsorption sites exist. This implies that larger ensembles of Pd exist in this sample as compared with 0.2Pd(Au) sample. This would correlate with the deposition of more than 1 layer of Pd on the Au core or with the formation of some monometallic Pd particles.

Following reduction, the 3.3Pd(Au) (Figure 10-c and f) sample displays the same bands as observed for 1.5Pd(Au) sample (2077, 2044 and 1936 cm^{-1}). This would, in principle, be consistent with a thicker Pd shell grown around a gold core. However, spectra collected after a treatment intended to remove PVP (Figure 11-c) suggests differently, given that a prominent band was observed at 2108 cm^{-1}. This band is attributed to CO adsorbed on Au-edge atoms and highlights that Au atoms definitely contribute to the surface sites. Given that this band is considerably more intense than for 0.2Pd(Au) sample it is thought that more of these sites exist for 3.3Pd(Au) sample. In order for this to be the case, less of the Au core must be covered by Pd. As a result it is highly likely that monometallic Pd particles exist within this sample. Lastly, the band associated with bridge bound CO on Pd edge sites is more pronounced for this sample (1975 cm^{-1}).

Discussion

0.2Pd(Au) sample

Detailed characterisation of the 0.2Pd(Au) material suggests that this sample is best described as an incomplete monolayer of Pd sitting on an Au core with a proposed structure presented in Figure 12. This structure appears close to the intended design and was likely possible due to the exceptionally slow Pd addition rate (5 µmol h^{-1}) which should minimise Pd solution concentration during synthesis – disfavouring the formation of monometallic Pd particles whilst favouring deposition of Pd onto pre-existing Au cores. Indeed, FTIR confirms the absence of monometallic Pd particles since there is no evidence of three-fold hollow adsorption sites (Figure 10-a and b, Figure 11-a). There are only weak bands associated with bridge bound CO (more evident after partial removal of PVP - Figure 11-a). Interestingly the removal of PVP did appear to uncover Pd-edge sites (1970 cm^{-1}), although these sites appeared to have little effect on catalytic performance (Table 2- entries 3, 4 and 5). The appearance of an absorption band associated with CO adsorbed on low coordinated Au sites[67,68] after PVP removal is consistent with incomplete coverage of the Au core (Figure 11-a). Combined TEM-EDS analysis of unsupported 0.2Pd(Au) nanoparticles tend to suggest that both metals were present together but with a consistently high Au and low Pd content suggesting good sample uniformity (Figure 4-a and b). Immobilisation of the 0.2Pd(Au) nanoparticles onto TiO_2 is not thought to have disrupted the structure with evidence a faint core-shell structure in a small minority of particles and no evidence of crystal lattice alignment between the nanoparticles and the support (i.e., no surface wetting) – see Figure 5.

Catalytic data collected for the selective hydrogenation of acetylene shows that 0.2Pd(Au) sample produces ethylene and oligomers as the major reaction products (Table 2 and Figure 9). This holds

true, irrespective of whether an attempt was made to remove residual surface PVP or not (Table 2 – entries 3, 4 and 5). The catalyst also shows remarkably low ethane selectivity even at temperatures well in excess of that necessary to fully react acetylene (i.e., under conditions where ethylene is free to adsorb and react). This is in contrast to a monometallic Pd catalyst which produces ethane as major product (Table 2 – entry 1). In principle, two explanations can be used to rationalise the low ethane selectivity of 0.2Pd(Au). Firstly, any Pd present is highly dispersed meaning that formation of the β-Pd-hydride phase is avoided.[65] Given that this phase is generally associated with ethane formation, its absence would account for decreased ethane formation/increased ethylene selectivity.[6,7,8,9,10,11,12,13,14,15,16] Secondly, since the amount of Pd present is insufficient to cover the Au core it is possible that Au acts as an additional reaction site. This could be as a result of direct hydrogenation on Au sites or *via* Pd assisted hydrogen dissociation (i.e., H_2 dissociation on Pd and spillover onto Au) as has been reported for CuPd catalysts[39,40,41,42] (and possibly for AgPd[47] and AuPd[48]). Regardless of the mechanism, the participation of Au would explain the relatively high oligomer selectivity and deactivation at lower temperature since both are characteristic traits of Au during alkyne hydrogenation,[38] especially at the low temperatures employed in this study. The involvement of Au as a reaction site may also contribute to low ethane selectivity given that ethylene adsorption on Au is an activated process (i.e., subject to an energy barrier).[38] These results also suggest that the interplay between Pd and Au may be further modified by changing the Pd surface coverage and may warrant further investigation. Low ethane selectivity is most likely associated with the combined effects of high Pd dispersion and the role of Au as a reaction site. However, given that the activity of 0.2Pd(Au) is far higher than that of monometallic Au, it would suggest that direct hydrogenation on Au is the least likely process to occur.

1.5Pd(Au) and 3.3Pd(Au) samples

Both 1.5Pd(Au) and 3.3Pd(Au) samples show similar catalytic performance with product distributions which favour ethane (Table 2 – entries 6 and 7, respectively) and closely mirror that of monometallic Pd (Table 2 - entry 1). That being the case, it is highly likely that both samples contain monometallic Pd nanoparticles, (formed due to the higher Pd addition rate – see Table 1) that act as the dominant reaction site during catalytic testing. Indeed, neither sample displays any evidence of deactivation (Supporting information figure 2 and 3) suggesting that Au is not an active site in either material (i.e., no surface Au sites exist or the activity of any exposed Au is significantly lower than Pd). Characterisation of the two samples suggests small but subtle differences with proposed structures presented in Figure 13. FTIR spectra of CO adsorbed on 1.5Pd(Au) shows no band at *ca*. 2100 cm^{-1} which suggests the absence of low coordinated Au sites (Figure 10-c and d, Figure 11-b). This may

imply that exposed Au atoms do not occupy low coordination sites, or that the pre-formed Au cores are completely covered in Pd. The later explanation is considered more plausible given that CO adsorption was apparent on Au for both 0.2Pd(Au) and 3.3Pd(Au) samples (Figure 11-b). That being the case, it is thought that some nanoparticles in 1.5Pd(Au) will possess a core-shell structure. In addition, TEM-EDS analysis showed that some Pd rich regions are present (Figure 4-d and e). As such, the 1.5Pd(Au) sample probably contains core-shell nanoparticles and monometallic Pd particles, with the latter type of particle being responsible for the catalytic activity and tendency to over-hydrogenate and form ethane. TEM images with elemental analysis of the 3.3Pd(Au) sample shows similar Pd rich regions (Figure 4-h). However, in this case, CO adsorption on Au is apparent (Figure 11-c), suggesting that at most, partial coverage of the Au core is possible (Figure 13). More pronounced bridging and three-fold hollow sites are thought to imply that monometallic Pd particles are more common for this sample. Overall, the differences between the three materials highlights that in-spite of a similar synthesis methodology, different nanostructures can form. This therefore requires detailed characterisation before useful links between catalytic performance and structure can be obtained.

Conclusions

It was shown that the addition of Pd to pre-formed Au nanoparticles under reducing conditions can selectively result in the deposition of Pd onto the Au core producing nanoparticles with core-shell morphology. The likelihood of this occurring was found to depend on the rate of Pd addition with slow addition favouring deposition onto Au, whereas faster addition allowed for the formation of monometallic Pd particles to form in addition to core-shell nanoparticles. In samples where monometallic Pd particles formed, these appeared to dominate catalytic performance favouring over-hydrogenation of acetylene to ethane. In one material – 0.2Pd(Au) – a partial Pd shell was grown onto the Au core and this material favoured ethylene and oligomers as major reaction products. High oligomer selectivity was attributed to the presence of exposed Au atoms which ultimately leads to deactivation. The high ethylene selectivity was attributed to the high dispersion of Pd which minimises the extent of β-Pd-hydride formation, although spillover of hydrogen from Pd to Au sites may also result in increased ethylene selectivity given that Au typically hydrogenates alkenes to a lesser extent. Overall, interesting catalytic performance can be obtained by careful synthesis of core-shell structures, however, the synthesis remains challenging and detailed characterisation is necessary to understand the nanostructures formed.

Acknowledgements

We thank the University of Aberdeen for financial support and Dr K. McManus (University of Aberdeen) for performing preliminary experiments with these samples. Electron microscopy and EDS were performed by RTB at the Electron Microscopy Facility, University of St Andrews.

Tables and Figures

Table 1: Chemical characteristics of the catalysts

Sample	Pd addition rate [µmol h^{-1}]	Nominal composition [wt%]		Nominal Pd:Au atomic ratio	Actual Pd:Au atomic ratio[a]	Average particle size[b] [nm]	CO uptake[c] [µmol g^{-1}]
		Pd	Au				
Pd	-	1.00	-	-	-	-	3.7
0.2Pd(Au)	5	0.10	0.91	0.2	0.26	3.5	2.2
1.5Pd(Au)	36	0.45	0.55	1.5	0.80	3.6	6.6
3.3Pd(Au)	57	0.65	0.37	3.2	1.10	3.7	5.3
Au	-	-	1.00	-	-	-	negligible

[a] Determined by EDS using TiO_2 supported samples

[b] Determined by TEM using TiO_2 supported samples

[c] Determined by CO pulse chemisorption

Table 2: Acetylene conversion and ethylene/ethane/oligomer selectivity over various catalysts at 363 K.

Entry	Sample	Conversion [%]	$S_{ethylene}$ [%]	S_{ethane} [%]	$S_{oligomers}$ [%]
1	Pd	100	23	55	22
2	Pd[a]	100	25	51	24
3	0.2Pd(Au)	100	53	6	41
4	0.2Pd(Au)[b]	100	53	7	40
5	0.2Pd(Au)[c]	100	52	9	39
6	1.5Pd(Au)	100	27	51	22
7	3.3Pd(Au)	100	25	50	25
8	Au	21	62	21	17

[a] Sample calcined at 673 K

[b] Sample was pre-treated by heating in water at 363 K to remove PVP

[c] Sample was pre-treated in water whilst exposed to UV light to remove PVP

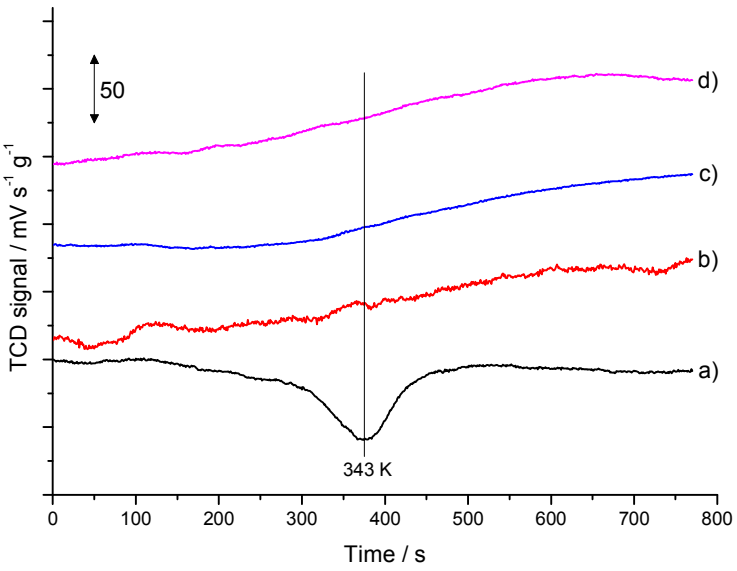

Figure 1 – TPR profiles for samples heated from 313 to 373 K at 5 K min^{-1}. (a) Pd, (b) 0.2Pd(Au), (c) 1.5 Pd(Au) and (d) 3.3 Pd(Au).

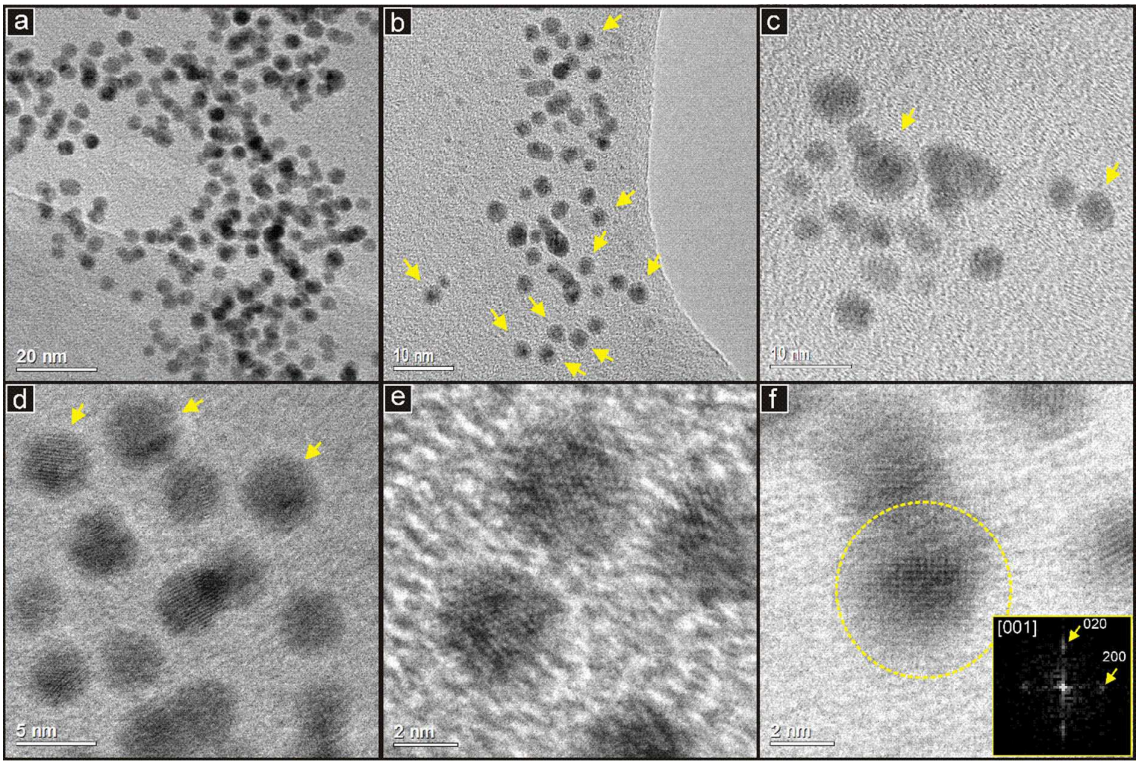

Figure 2 - TEM images of unsupported 3.3Pd(Au) nanoparticles at a range of magnifications. The DDP of the nanoparticle circled in image (f) is inset. Particles with apparent core-shell morphology are indicated. See text for further details of all TEM figures.

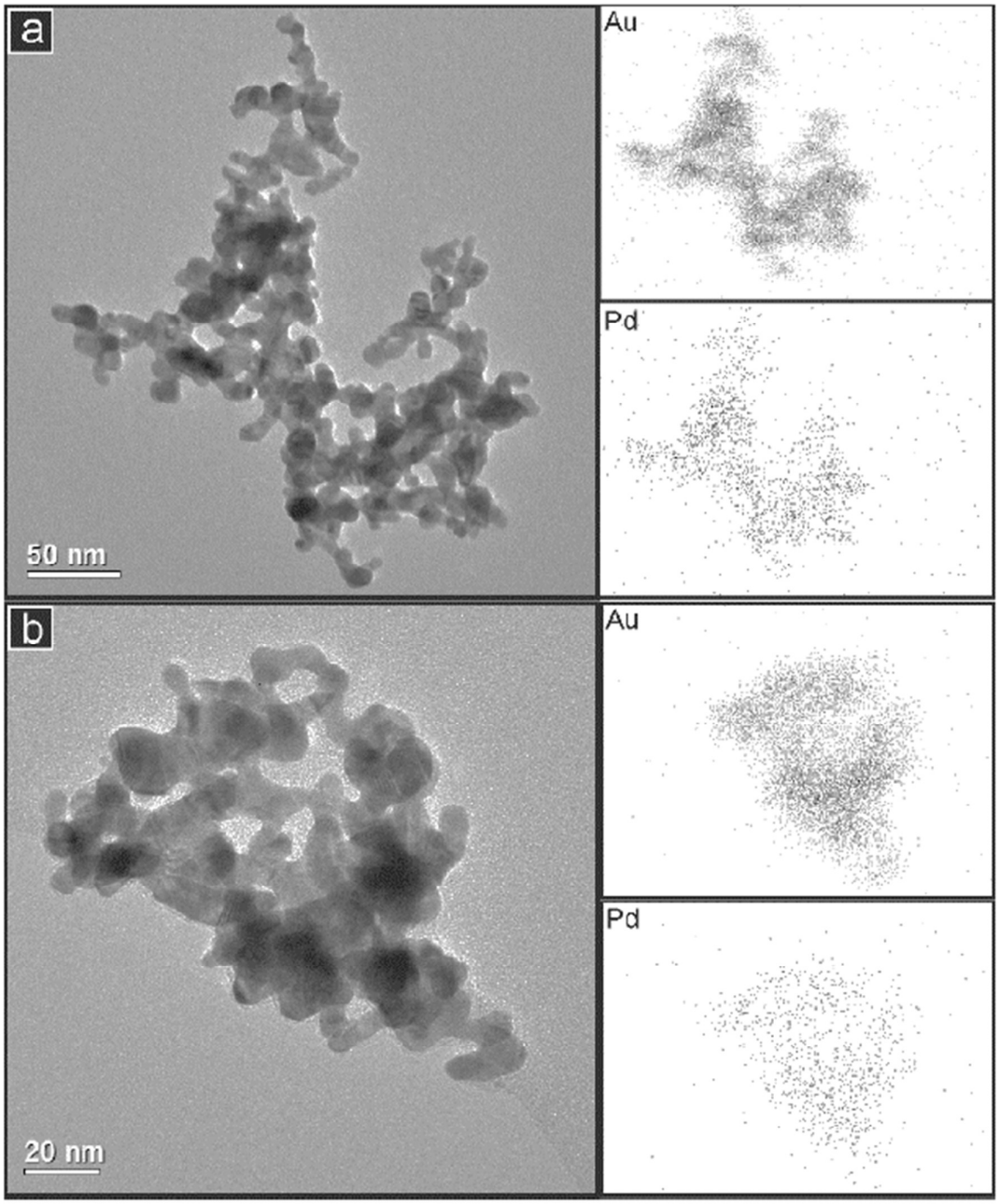

Figure 3 - TEM images of two groups of unsupported 3.3Pd(Au) nanoparticles (after centrifugation) along with the corresponding EDS elemental maps for Au and Pd.

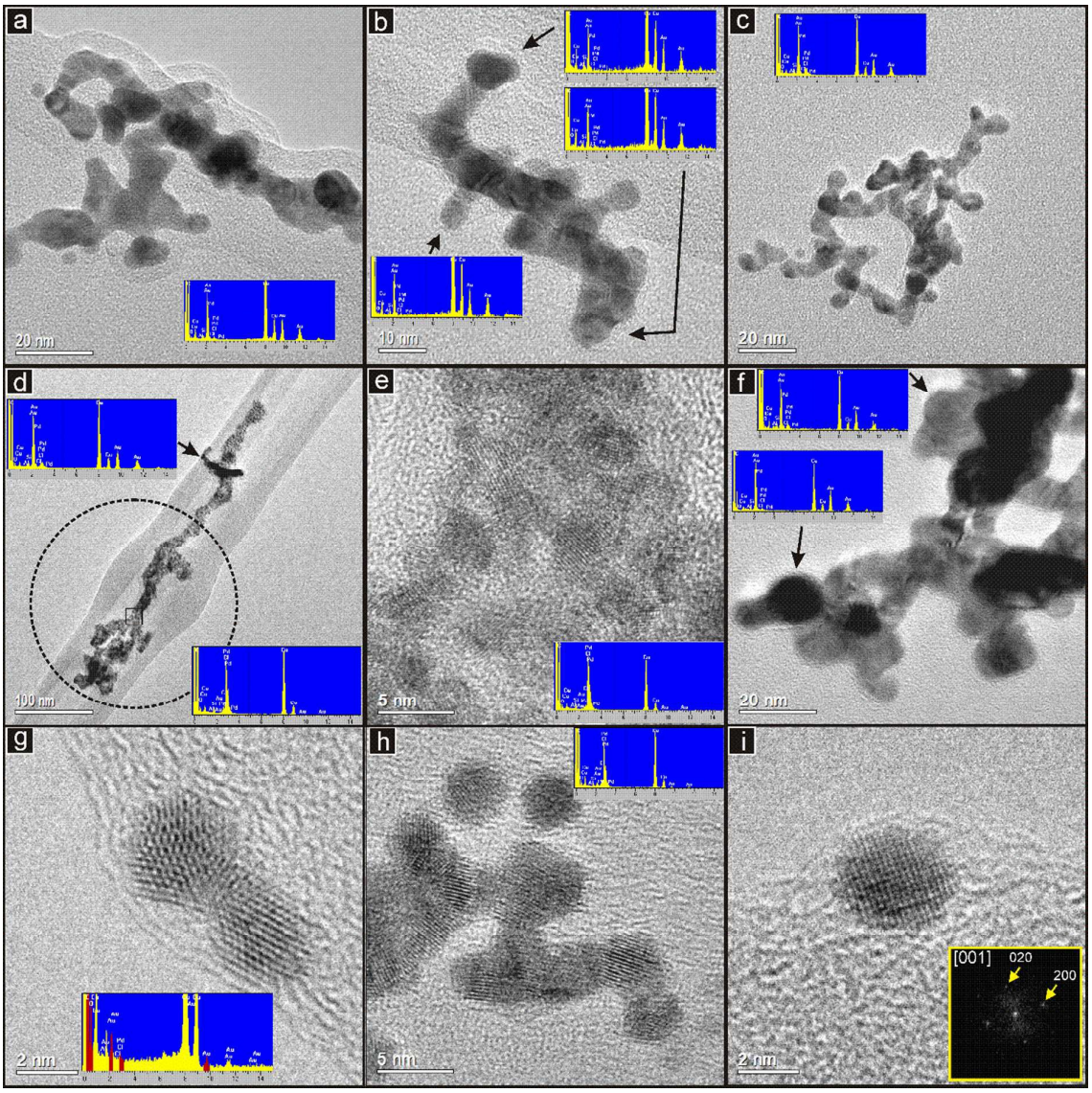

Figure 4 - TEM images of unsupported nanoparticles (after centrifugation) with corresponding EDS spectra. Spectra are of the whole field of view, the circled area in (d) or the regions indicated with arrows. Images (a) and (b) show 0.2Pd(Au) nanoparticles, (c) to (e) show 1.5Pd(Au) nanoparticles and (f) to (i) show 3.3Pd(Au) nanoparticles. The DDP of the nanoparticle in image (i) is inset. Image (e) is an expanded view of the small square are in image (d).

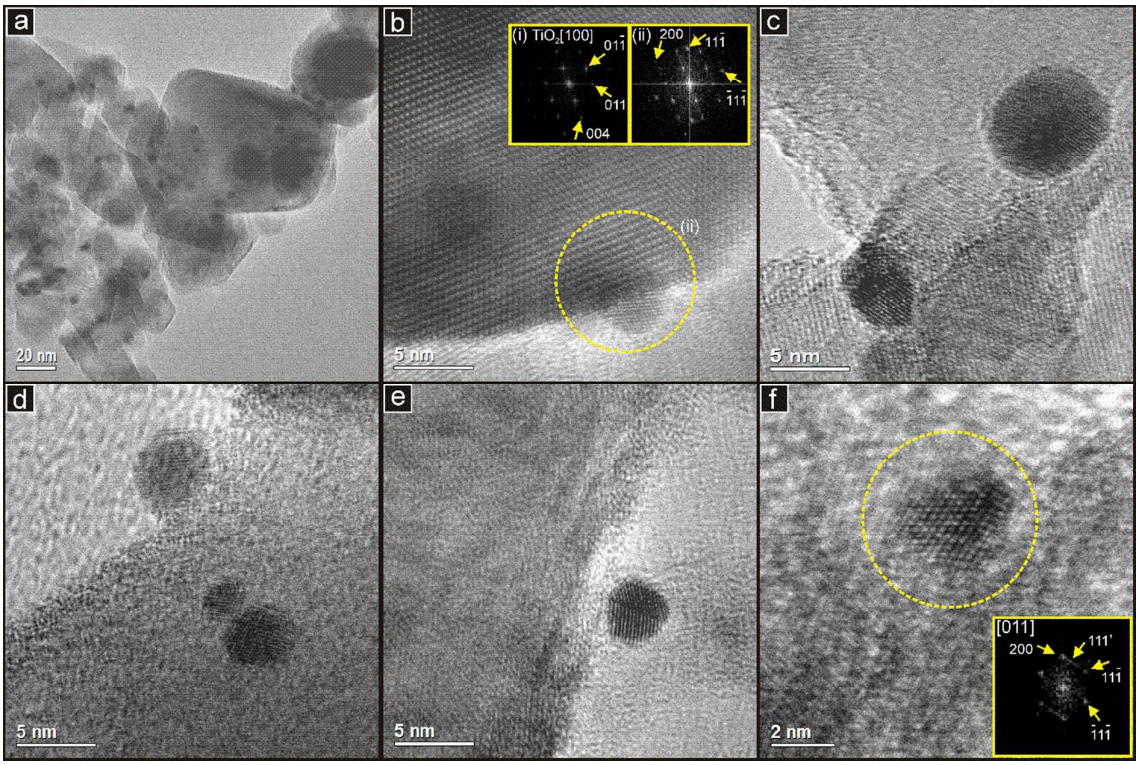

Figure 5 - TEM images of 0.2Pd(Au) nanoparticles supported on TiO_2 at a range of magnifications. Image (b) includes the DDP of (i) the support which is indexed to anatase and (ii) the metal nanoparticle and support (circled). The DDP of the twinned nanoparticle (circled) in image (f) shows a full diffraction pattern relating to the larger crystal domain (LHS) and additional spots (') from the smaller domain (RHS).

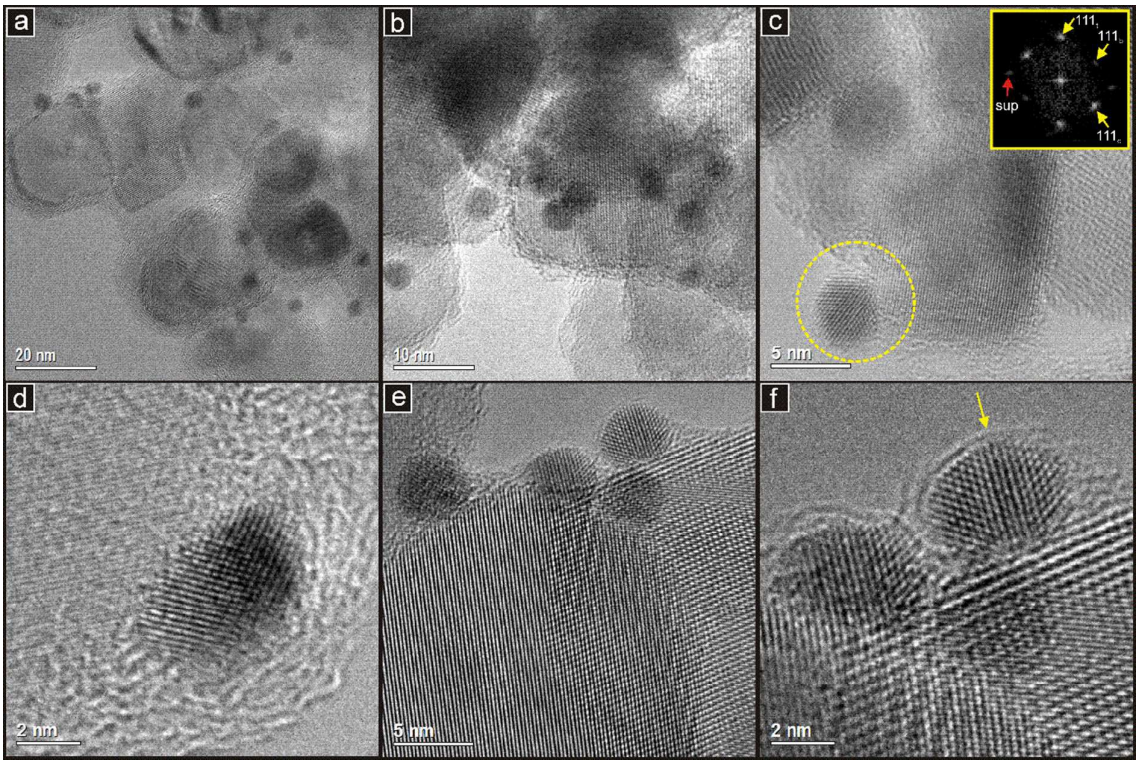

Figure 6 - TEM images of 1.5Pd(Au) nanoparticles supported on TiO_2 at a range of magnifications. The DDP of the nanoparticle circled in image (c) is inset. Spots due to two crystal domains in the nanoparticle (t=top, b=bottom, c=common to both domains) and the oxide support (sup) are indicated. Image (f) is an expanded view from (e) in which the twin boundary of one nanoparticle is indicated

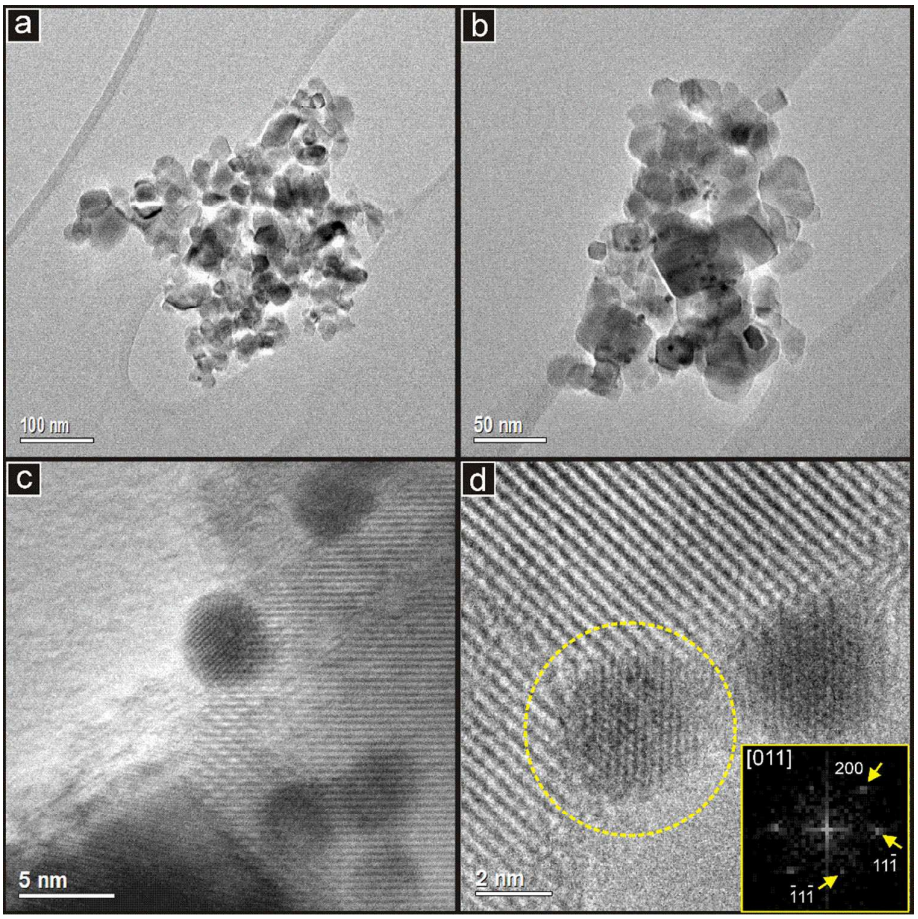

Figure 7 - TEM images of 3.3Pd(Au) nanoparticles supported on TiO_2 at a range of magnifications. The DDP of the nanoparticle circled in image (d) is inset.

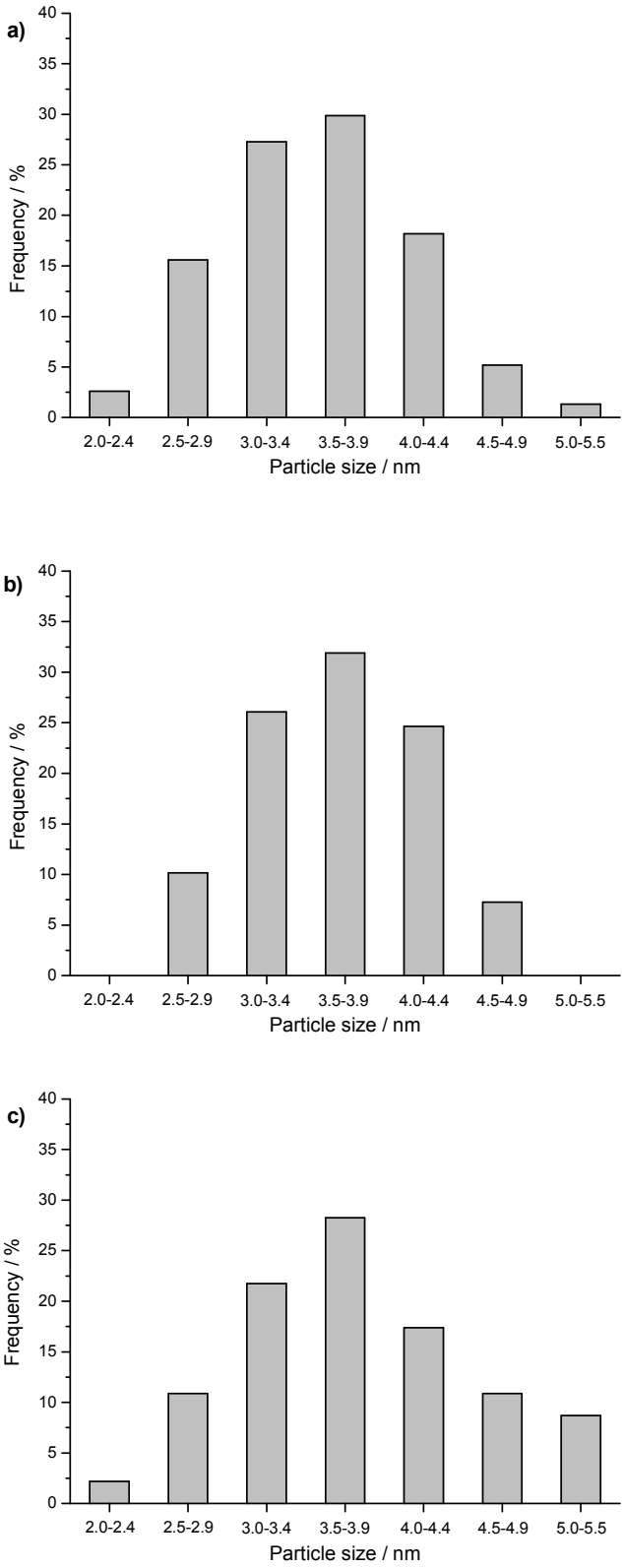

Figure 8 – Metal nanoparticle size distributions determined by TEM for a) 0.2Pd(Au), b) 1.5Pd(Au) and c) 3.3Pd(Au).

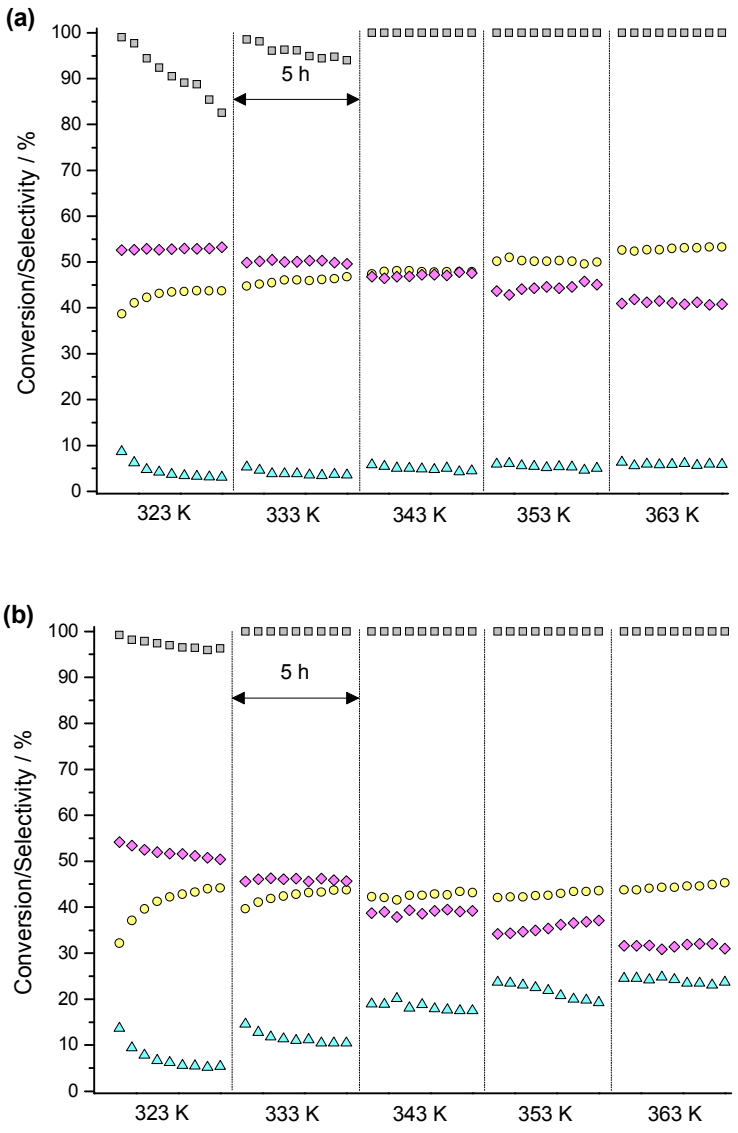

Figure 9 – Time on stream data (5 h periods) for 0.2Pd(Au) for at temperature between 323-363 K using H_2: acetylene ratios of (a) 1.8:1 and (b) 3.6:1. Acetylene conversion (grey squares), ethylene selectivity (yellow circles), ethane (cyan triangles) and oligomer selectivity (pink diamonds).

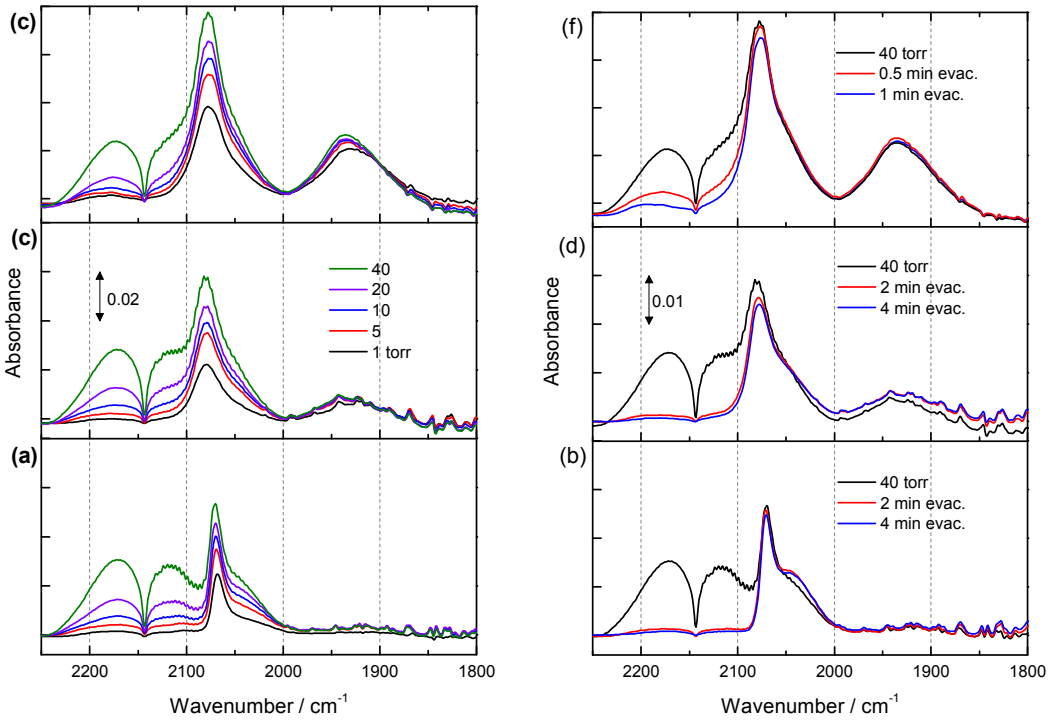

Figure 10. FTIR spectra of samples after reduction at 373 K exposure to CO at room temperature. (a) 0.2Pd(Au), (b) 0.2Pd(Au) after evacuation, (c) 1.5Pd(Au), (d) 1.5Pd(Au) after evacuation, 3.3Pd(Au) and (f) 3.3Pd(Au) after evacuation.

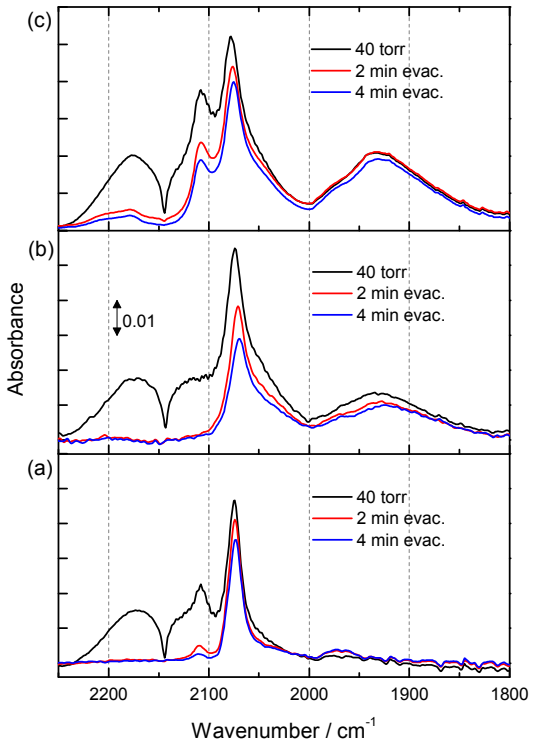

Figure 11 - FTIR spectra of samples exposed to UV irradiation after reduction at 373 K exposure to CO at room temperature and subsequent evacuation. (a) 0.2Pd(Au), (b) 1.5Pd(Au) and (c) 3.3Pd(Au).

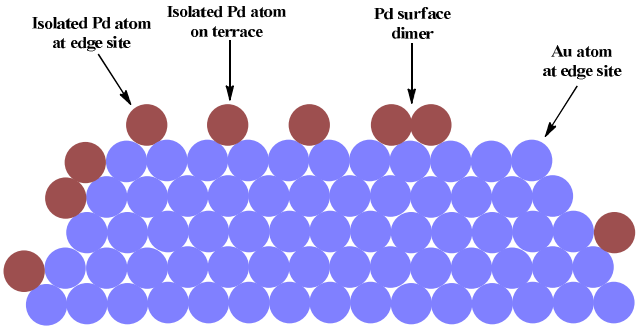

Figure 12 – Proposed structure of 0.2Pd(Au) after removal of PVP

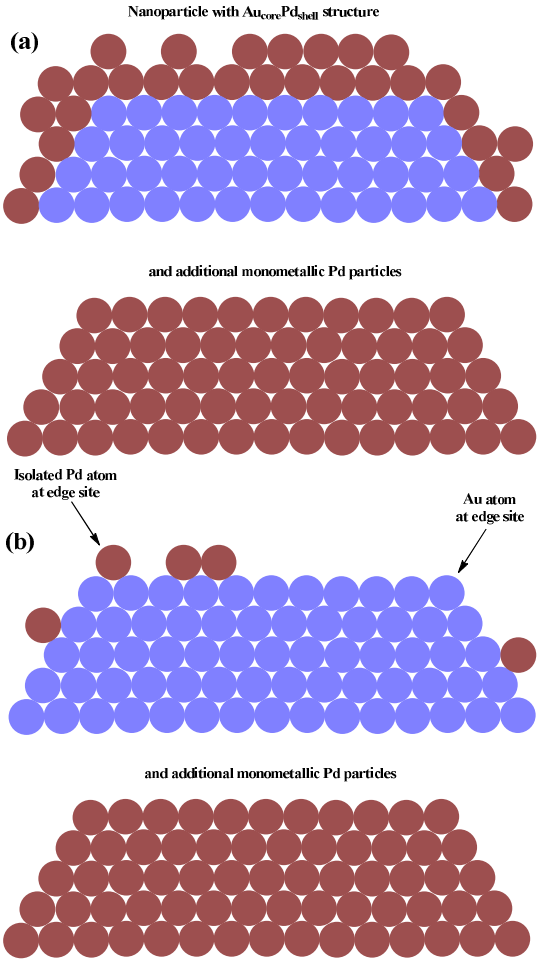

Figure 13 - Proposed structure of (a) 1.5Pd(Au) and (b) 3.3Pd(Au)

Supporting information

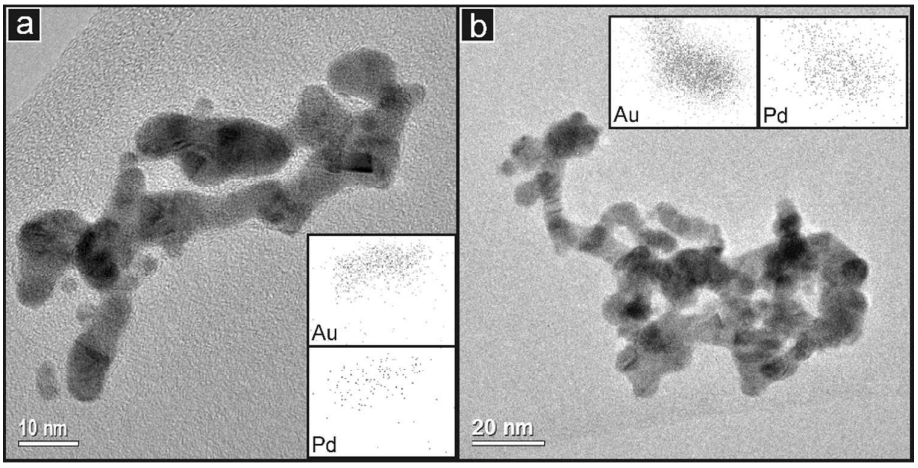

Supporting information figure 1 - TEM images of groups of unsupported 1.5Pd(Au) nanoparticles (after centrifugation) along with the corresponding EDS elemental maps for Au and Pd.

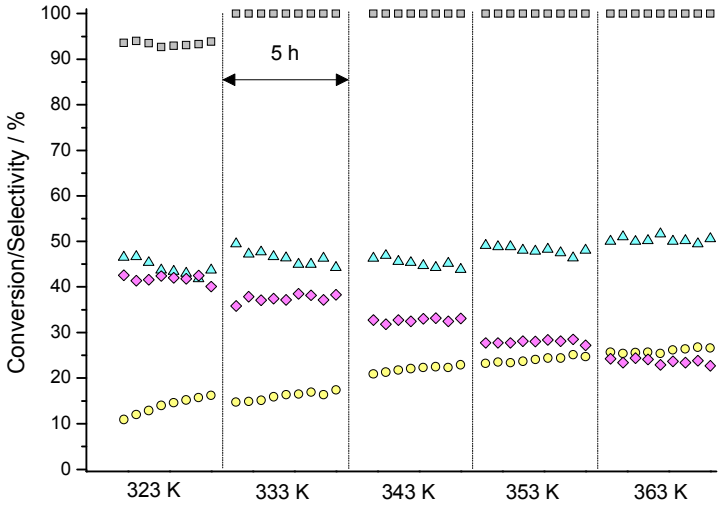

Supporting information figure 2 - Time on stream data (5 h periods) for 1.5Pd(Au) for at temperature between 323-363 K using a H_2: acetylene ratio of 1.8:1. Acetylene conversion (grey squares), ethylene selectivity (yellow circles), ethane (cyan triangles) and oligomer selectivity (pink diamonds).

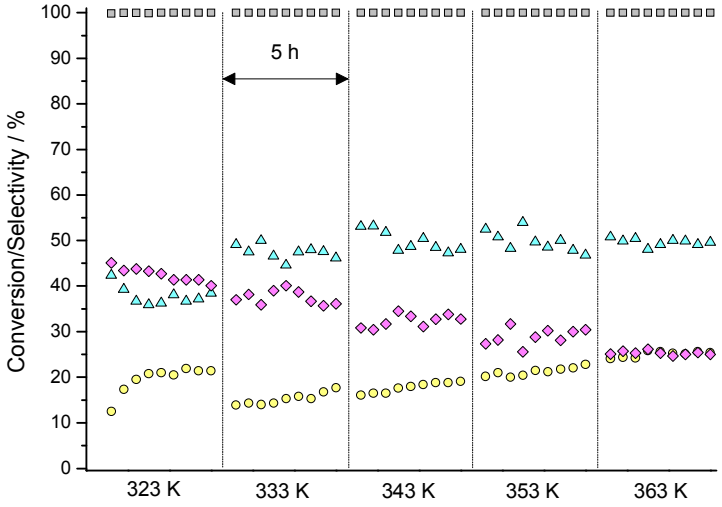

Supporting information figure 3 - Time on stream data (5 h periods) for 3.3Pd(Au) for at temperature between 323-363 K using a H_2: acetylene ratio of 1.8:1. Acetylene conversion (grey squares), ethylene selectivity (yellow circles), ethane (cyan triangles) and oligomer selectivity (pink diamonds).

References

[1] A. Borodziński and G. C. Bond, *Catal. Rev.*, 2006, **48**, 91–144.
[2] A. Borodziński and G. C. Bond, Catal. Rev., 2008, **50**, 379-469.
[3] S. A. Nikolaev, I. L. N. Zanaveskin, V. V Smirnov, V. A. Averyanov and K. I. Zanaveskin, *Russ. Chem. Rev.*, 2009, **78**, 231–247.
[4] D. B. Tiedtke, t. T. P. Cheung, J. Leger, S. A. Zisman, J. J. Bergmeister and G. A. Delzer in: *13th Ethlyene Producers Conference*, 2001, **10**, p. 1.
[5] G. C. Bond and P. B. Wells, *Advances in Catalysis*, 1964, **15**, 91-226.
[6] D. Teschner, J. Borsodi, A. Wootsch, Z. Révay, M. Hävecker, A. Knop-Gericke, S. D. Jackson and R. Schlögl, *Science*, 2008, **320**, 86–89.
[7] D. Teschner, J. Borsodi, Z. Kis, L. Szentmiklósi, Z. Révay, A. Knop-Gericke, R. Schlögl, D. Torres and P. Sautet, *J. Phys. Chem. C*, 2010, **114**, 2293–2299.
[8] M. Armbrüster, M. Behrens, F. Cinquini, K. Föttinger, Y. Grin, A. Haghofer, B. Klötzer, A. Knop-Gericke, H. Lorenz, A. Ota, S. Penner, J. Prinz, C. Rameshan, Z. Révay, D. Rosenthal, G. Rupprechter, P. Sautet, R. Schlögl, L. Shao, L. Szentmiklósi, D. Teschner, D. Torres, R. Wagner, R. Widmer and G. Wowsnick, *ChemCatChem*, 2012, **4**, 1048–1063.
[9] M. García-Mota, B. Bridier, J. Pérez-Ramírez and N. López, *J. Catal.*, 2010, **273**, 92–102.
[10] B. Bridier, N. Lopez and J. Pérez-Ramírez, *Dalt. Trans.*, 2010, **39**, 8412–8419.
[11] W. Ludwig, A. Savara, K. H. Dostert and S. Schauermann, *J. Catal.*, 2011, **284**, 148–156.
[12] W. Ludwig, A. Savara, R. J. Madix, S. Schauermann and H. J. Freund, *J. Phys. Chem. C*, 2012, **116**, 3539–3544.
[13] S. Schauermann, N. Nilius, S. Shaikhutdinov and H. J. Freund, *Acc. Chem. Res.*, 2013, **46**, 1673–1681.
[14] J. Sá, G. D. Arteaga, R. A. Daley, J. Bernardi and J. A. Anderson, *J. Phys. Chem. B*, 2006, **110**, 17090–17095.
[15] B. Yang, R. Burch, C. Hardacre, G. Headdock and P. Hu, *J. Catal.*, 2013, **305**, 264–276.
[16] N. A. Khan, S. Shaikhutdinov and H. J. Freund, *Catal. Letters*, 2006, **108**, 159–164.
[17] A. J. McCue and J. A. Anderson, *Front. Chem. Sci. Eng.*, 2015, **9**, 142–153.
[18] A. D. Benavidez, P. D. Burton, J. L. Nogales, A. R. Jenkins, S. a. Ivanov, J. T. Miller, A. M. Karim and A. K. Datye, *Appl. Catal. A Gen.*, 2014, **482**, 108–115.
[19] Y. K. Gulyaeva, V. V. Kaichev, V. I. Zaikovskii, E. V. Kovalyov, A. P. Suknev and B. S. Bal'zhinimaev, *Catal. Today*, 2015, **245**, 139–146.
[20] S. A. Nikolaev and V. V. Smirnov, *Catal. Today*, 2009, **147S**, S336–S341.
[21] S. A. Nikolaev, V. V. Smirnov, A. Y. Vasil'kov and V. L. Podshibikhin, *Kinet. Catal.*, 2010, **51**, 375–379.
[22] B. Bridier and J. Pérez-Ramírez, *J. Am. Chem. Soc.*, 2010, **132**, 4321–4327.
[23] F. M. McKenna, R. P. K. Wells and J. A. Anderson, *Chem. Commun.*, 2011, **47**, 2351–2353.
[24] A. J. McCue, F.-M. McKenna and J. A. Anderson, *Catal. Sci. Technol.*, 2015, **5**, 2449–2459.
[25] F. M. McKenna and J. A. Anderson, *J. Catal.*, 2011, **281**, 231–240.
[26] F. M. McKenna, L. Mantarosie, R. P. K. Wells, C. Hardacre and J. a. Anderson, *Catal. Sci. Technol.*, 2012, **2**, 632–638.
[27] A. J. McCue and J. A. Anderson, *Catal. Sci. Technol.*, 2014, **4**, 272–294.
[28] F. Studt, F. Abild-Pedersen, T. Bligaard, R. Z. Sørensen, C. H. Christensen and J. K. Nørskov, *Angew. Chemie Int. Ed.*, 2008, **47**, 9299–9302.
[29] S. K. Kim, J. H. Lee, I. Y. Ahn, W. J. Kim and S. H. Moon, *Appl. Catal. A Gen.*, 2011, **401**, 12–19.

[30] M. Friedrich, S. A. Villaseca, L. Szentmiklósi, D. Teschner and M. Armbrüster, *Materials*, 2013, **6**, 2958–2977.
[31] J. Osswald, R. Giedigkeit, R. E. Jentoft, M. Armbrüster, G. F, K. Kovnir, R. Thorsten, Y. Grin and R. Schlögl, *J. Catal.*, 2008, **258**, 210–218.
[32] J. Osswald, K. Kovnir, M. Armbrüster, R. Giedigkeit, R. E. Jentoft, U. Wild, Y. Grin and R. Schlögl, *J. Catal.*, 2008, **258**, 219–227.
[33] G. Vilé, D. Albani, M. Nachtegaal, Z. Chen, D. Dontsova, M. Antonietti, N. López and J. Pérez-Ramírez, *Angew. Chemie Int. Ed.*, 2015, **54**, 11265–11269.
[34] B. Bridier, N. López and J. Pérez-Ramírez, *J. Catal.*, 2010, **269**, 80–92.
[35] B. Bridier, M. a G. Hevia, N. López and J. Pérez-Ramírez, *J. Catal.*, 2011, **278**, 167–172.
[36] G. Vilé, D. Baudouin, I. N. Remediakis, C. Copéret, N. López and J. Pérez-Ramírez, *ChemCatChem*, 2013, **5**, 3750–3759.
[37] E. Oakton, G. Vilé, D. S. Levine, E. Zocher, D. Baudouin, J. Pérez-Ramírez and C. Copéret, *Dalt. Trans.*, 2014, **43**, 15138–15142.
[38] Y. Segura, N. López and J. Pérez-Ramírez, *J. Catal.*, 2007, **247**, 383–386.
[39] A. J. McCue, C. J. McRitchie, A. M. Shepherd and J. A. Anderson, *J. Catal.*, 2014, **319**, 127–135.
[40] A. J. McCue, A. M. Shepherd and J. A. Anderson, *Catal. Sci. Technol.*, 2015, **5**, 2880–2890.
[41] A. J. McCue and J. A. Anderson, *J. Catal.*, 2015, **329**, 538–546.
[42] A. J. McCue, A. Gibson and J. A. Anderson, *Chem. Eng. J.*, 2016, **285**, 384-391.
[43] H. L. Tierney, A. E. Baber, J. R. Kitchin and E. C. H. Sykes, *Phys. Rev. Lett.*, 2009, **103**, 246102–1–246102–4.
[44] G. Kyriakou, M. B. Boucher, A. D. Jewell, E. ALewis, T. J. Lawton, A. E. Baber, H. L. Tierney, M. Flytzani-stephanopoulos and E. C. H. Sykes, *Science (80-.).*, 2012, **335**, 1209–1212.
[45] M. B. Boucher, B. Zugic, G. Cladaras, J. Kammert, M. D. Marcinkowski, T. J. Lawton, E. C. H. Sykes and M. Flytzani-Stephanopoulos, *Phys. Chem. Chem. Phys.*, 2013, **15**, 12187–12196.
[46] Q. Fu and Y. Luo, *ACS Catal.*, 2013, **3**, 1245–1252.
[47] G. Pei, X. Liu, A. Wang, A. F. Lee, M. A Isaacs, L. Li, X. Pan, X. Yang, X. Wang, Z. Tai, K. Wilson and T. Zhang, *ACS Catal.*, 2015, **5**, 3717–3725.
[48] G. X. Pei, X. Y. Liu, A. Wang, L. Li, Y. Huang, T. Zhang, J. W. Lee, B. W. L. Jang and C.-Y. Mou, *New J. Chem.*, 2014, **38**, 2043–2051.
[49] G. Vilé, B. Bridier, J. Wichert and J. Pérez-Ramírez, *Angew. Chemie - Int. Ed.*, 2012, **51**, 8620–8623.
[50] G. Vilé, P. Dähler, J. Vecchietti, M. Baltanás, S. Collins, M. Calatayud, A. Bonivardi and J. Pérez-Ramírez, *J. Catal.*, 2015, **324**, 69–78.
[51] G. J. Hutchings and C. J. Kiely, *Acc. Chem. Res.*, 2013, **46**, 1759–1772.
[52] P. Paalanen, B. M. Weckhuysen and M. Sankar, *Catal. Sci. Technol.*, 2013, **3**, 2869–2880.
[53] C. Ma, Y. Du, J. Feng, X. Cao, J. Yang and D. Li, *J. Catal.*, 2014, **317**, 263–271.
[54] R. G. Chaudhuri and S. Paria, *Chem. Rev.*, 2012, **112**, 2373–2433.
[55] Q. Zhang, I. Lee, J. B. Joo, F. Zaera and Y. Yin, *Acc. Chem. Res.*, 2013, **46**, 1816–1824.
[56] Y. Mizukoshi, K. Sato, J. Kugai, T. a. Yamamoto, T. J. Konno and N. Masahashi, *J. Exp. Nanosci.*, 2013, **10**, 235–247.
[57] H. Wang, C. Wang, H. Yan, H. Yi and J. Lu, *J. Catal.*, 2015, **324**, 59–68.
[58] W. Jones, R. Su, P. P. Wells, Y. Shen, N. Dimitratos, M. Bowker, D. Morgan, B. B. Iversen, A. Chutia, F. Besenbacher and G. Hutchings, *Phys. Chem. Chem. Phys.*, 2014, **16**, 26638–26644.
[59] R. Tiruvalam, J. Pritchard, N. Dimitratos, J. Lopez-Sanchez, J. Edwards, A. Carley, G. Hutchings and C. Kiely, *Faraday Discuss.*, 2011, **152**, 63–86.
[60] P. T. Witte, P. H. Berben, S. Boland, E. H. Boymans, D. Vogt, J. W. Geus and J. G. Donkervoort, *Top. Catal.*, 2012, **55**, 505–511.
[61] P. T. Witte, S. Boland, F. Kirby, R. vanMaanen, B. F. Bleeker, D. a M. deWinter, J. a. Post, J. W. Geus and P. H. Berben, *ChemCatChem*, 2013, **5**, 582–587.

[62] M. Crespo-Quesada, J. M. Andanson, A. Yarulin, B. Lim, Y. Xia and L. Kiwi-Minsker, *Langmuir*, 2011, **27**, 7909–7916.
[63] J. A Lopez-Sanchez, N. Dimitratos, C. Hammond, G. L. Brett, L. Kesavan, S. White, P. Miedziak, R. Tiruvalam, R. L. Jenkins, A. F. Carley, D. Knight, C. J. Kiely and G. J. Hutchings, *Nat. Chem.*, 2011, **3**, 551–556.
[64] A. R. Wilson, K. Sun, M. Chi, R. M. White, J. M. Lebeau, H. H. Lamb and B. J. Wiley, *J. Phys. Chem. C*, 2013, **117**, 17557–17566.
[65] M. Boudart and H. S. Hwang, *J. Catal.*, 1975, **39**, 44–52.
[66] T. Lear, R. Marshall, J. A. Lopez-Sanchez, S. D. Jackson, T. M. Klapötke, M. Bäumer, G. Rupprechter, H.-J. Freund and D. Lennon, *J. Chem. Phys.*, 2005, **123**, 174706–1–13.
[67] R. Meyer, C. Lemire, S. K. Shaikhutdinov and H.-J. Freund, *Gold Bull.*, 2004, **37**, 72–124.
[68] Y. Zhu, J. He, C. Shang, X. Miao, J. Huang, Z. Liu, H. Chen and Y. Han, *J. Am. Chem. Soc.*, 2014, **136**, 12746–12752.
[69] B. Zhu, G. Thrimurthulu, L. Delannoy, C. Louis, C. Mottet, J. Creuze, B. Legrand and H. Guesmi, *J. Catal.*, 2013, **308**, 272–281.